PHYSICAL REVIEW A VOLUME 23, NUMBER 1 JANUARY 1981

Photoexcitation and ionization in carbon dioxide: Theoretical studies in the separated-channel static-exchange approximation

N. Padial and G. Csanak
Instituto de Fisica, Universidade Estadual de Campinas, Campinas, Brazil

B. V. McKoy
A. A. Noyes Laboratory of Chemical Physics, California Institute of Technology, Pasadena, California 91125

P. W. Langhoff
Department of Chemistry, Indiana University, Bloomington, Indiana 47405*
and Computational Chemistry Group, NASA Ames Research Center, Moffett Field, California 94035
(Received 21 April 1980)

Theoretical studies are reported of total and partial-channel photoexcitation and ionization cross sections in carbon dioxide. As in previously reported studies of discrete and continuum dipole spectra in diatomic (N_2, CO, O_2, F_2) and polyatomic (H_2O, H_2CO, O_3) molecules in this series, separated-channel static-exchange calculations of vertical-electronic transition energies and oscillator strengths and Stieltjes-Tchebycheff moment methods are employed in the development. Detailed comparisons are made of the static-exchange excitation and ionization spectra with photoabsorption, electron-impact excitation, and quantum-defect estimates of discrete transition energies and intensities, and with partial-channel photoionization cross sections obtained from fluorescence measurements and from tunable-source and $(e,2e)$ photoelectron spectroscopy. The spectral characteristics of the various discrete series and continua are interpreted in terms of contributions from compact $2\pi_u$ (π^*), $5\sigma_g$ (σ^*), and $4\sigma_u$ (σ^*) virtual valence orbitals, and from more diffuse discrete and continuum Rydberg orbitals. The $2\pi_u$ (π^*) orbital is found to contribute to discrete excitation series, whereas the $5\sigma_g$ (σ^*) and $4\sigma_u$ (σ^*) orbitals generally appear in the photoionization continua as resonancelike diabatic valence features. Good agreement obtains between the calculated discrete excitation series and the results of a recent analysis of the available spectroscopic data. The calculated outer-valence-shell $(1\pi_g^{-1})X\,^2\Pi_g$, $(1\pi_u^{-1})A\,^2\Pi_u$, $(3\sigma_u^{-1})B\,^2\Sigma_u^+$, and $(4\sigma_g^{-1})C\,^2\Sigma_g^+$ partial-channel photoionization cross sections are in good accord with measured values, and clarify completely the origins of the various structures in the observed spectra. There is evidence, however, of coupling among scattering states associated with $1\pi_g^{-1}$ and $1\pi_u^{-1}$ ionic channels, giving rise to moderate disagreement with tunable-source photoelectron and fluorescence measurements over a portion of the spectrum. In the inner-valence-shell region, the calculated $2\sigma_u^{-1}$ and $3\sigma_g^{-1}$ cross sections are in qualitative accord with the observed many-electron spectral intensities, and provide a basis for quantitative interpretation when combined with appropriate intensity-borrowing calculations. The calculated carbon and oxygen K-edge cross sections are in good agreement with available cross sections obtained from electron-impact and photoabsorption measurements. It is of particular interest to find the oxygen K-edge ($1\sigma_g^{-1}$, $1\sigma_u^{-1}$) cross section exhibits both the expected $5\sigma_g$ (σ^*) and $4\sigma_u$ (σ^*) resonancelike features. Finally, comparisons are made throughout of the discrete and continuum spectra in carbon dioxide with the results of previously reported studies in CO and O_2, and the origins of the similarities and differences in the cross sections in these cases are clarified.

I. INTRODUCTION

Photoabsorption and related optical processes in carbon dioxide have been subjects of continuing experimental and theoretical study. The various experimental investigations reported include spectroscopic and photoabsorption,[1-16] electron-impact excitation,[17-19] and photoelectron spectral[20-28] measurements. More recently, total and partial-channel photoionization cross sections have been studied employing dipole and binary $(e,2e)$ and $(e,e+\text{ion})$ spectroscopy,[29-31] synchrotron and bremsstrahlung radiation sources,[32-34] fluorescence yields,[35-37] and line-source measurements of branching ratios.[38-41] Moreover, the ground and certain of the excited electronic states in carbon dioxide have been studied theoretically employing Hartree-Fock (HF),[42-45] random-phase-approximation (RPA),[46] configuration-interaction,[47-50] and semi-empirical[51,52] techniques. Final-ionic-state amplitudes useful for assigning photoelectron spectra have also been obtained from recent Green's function calculations.[53-55] However, aside from very approximate estimates,[56] theoretical investigations of partial-channel photoionization cross sections in CO_2 have apparently not been reported. Studies of the far uv dipole excitation and ionization spectra in carbon dioxide that clarify and complement the available experimental data would clearly be desirable.

In the present article, theoretical studies of vertical-electronic dipole excitation and ionization spectra in CO_2 are reported. The procedures and approximations employed follow closely those of previously reported studies in diatomic (N_2, CO, O_2, F_2) and polyatomic (H_2O, H_2CO, O_3) molecules in this series.[57-68] Specifically, L^2 static-exchange calculations and Stieltjes-Tchebycheff moment-theory techniques[69,70] are employed, allowing for discussion and clarification of both discrete and continuum spectra for all nine occupied canonical molecular orbitals in carbon dioxide from a common perspective. Use of canonical HF orbitals ensures that appropriate ionic states and static-exchange $V^{(N-1)}$ potentials are incorporated in the development, in accordance with Koopmans theorem. Previous experience indicates the static-exchange results so obtained provide useful first approximations to outer-valence-shell and K-edge cross sections in light diatomic and polyatomic molecules.[57-67] Moreover, when supplemented with appropriate ionic-state intensity-borrowing calculations, the static-exchange spectra also provide results in good accord with inner-valence-shell cross sections.[68] Finally, ionic-fragment and molecular-ion yields can be obtained from the static-exchange calculations by incorporating the necessary Franck-Condon factors, and non-Franck-Condon effects can be investigated, if necessary, by explicitly incorporating the vibrational degrees of freedom. These latter aspects of photoionization studies are not included in the present development, however.

The outer-valence-shell $1\pi_g$ (n), $1\pi_u$ (π), $3\sigma_u$ (σ), and $4\sigma_g$ (σ) excitation spectra are found to be comprised of Rydberg series and intense intravalence transitions involving the $2\pi_u$ (π^*) virtual orbital which are in good quantitative accord with recently reported spectral assignments.[52] There is also an intense $1\pi_u \rightarrow 5\sigma_g$ (σ^*) intravalence transition in the calculated static-exchange spectrum which may contribute to photoproduction of CO in the $A\,^1\Pi_u$ state.[18] The $1\pi_g$ and $1\pi_u$ partial-channel photoionization cross sections are dominated by $2p \rightarrow kd$ features of largely atomiclike origin, whereas the $3\sigma_u$ and $4\sigma_g$ cross sections include strong resonancelike intravalence diabatic transitions into $5\sigma_g$ (σ^*) and $4\sigma_u$ (σ^*) virtual orbitals, respectively. These results clarify fully the origins of the various structures in the measured outer-valence-shell partial-channel cross sections. Modest quantitated discrepancies between theory and experiment for the $X\,^2\Pi_g$ and $A\,^2\Pi_u$ channels are tentatively attributed to the effects of scattering-state coupling. The calculations also provide a separation of the overlapping $A\,^2\Pi_u$ and $B\,^2\Sigma_u^+$ channels not achieved by photoelectron spectroscopy, and allow for comparison with fluorescence measurements of the $A\,^2\Pi_u/B\,^2\Sigma_u^+$ ratio. The inner-valence-shell $2\sigma_u$ (σ) and $3\sigma_g$ (σ) cross sections are found to exhibit $5\sigma_g$ (σ^*) and $4\sigma_u$ (σ^*) photoionization resonances, respectively, and their intensities are in general accord with the measured many-electron ionization cross section in this spectral interval, although there is some evidence of scattering-state coupling with the $(4\sigma_g^{-1})C\,^2\Sigma_g^+$ channel. Finally, the calculated $2\sigma_g$ (C1s) and $1\sigma_u$ (O1s), $1\sigma_g$ (O1s) K-edge cross sections are found to be in excellent accord with recent electron-impact and photoabsorption studies, and clarify the origins of the resonance features observed above the ionization thresholds in these cases.[19,32,34] It is of particular interest to note that both $5\sigma_g$ (σ^*) and $4\sigma_u$ (σ^*) features appear in the calculated O1s K-edge cross section, in good accord with the measured profile.

The static-exchange calculations performed using L^2 Gaussian basis sets and the moment-theory development are described in Sec. II, the partial-channel excitation series and photoionization cross sections in CO_2 are presented in Sec. III, and concluding remarks are made in Sec. IV.

II. STATIC-EXCHANGE AND MOMENT-THEORY CALCULATIONS IN CO_2

In this section a brief descriptive account is given of the L^2 static-exchange approximation employed in the present development and of the moment-theory approach used to construct the corresponding photoionization cross sections.[69,70]

A Hartree-Fock function is constructed at the experimental equilibrium geometry (C–O length $=2.1944a_0$) in CO_2 employing a $(10s, 5p)/[3s, 2p]$ Gaussian basis set and appropriate computational methods.[71,72] The resulting canonical Hartree-Fock molecular orbitals are used in forming static-exchange Hamiltonians

$$h_\gamma = T + V + V_\gamma \ , \tag{1a}$$

$$V_\gamma = \sum_i 2a_i^\gamma \hat{J}_i - b_i^\gamma \hat{K}_i \ , \tag{1b}$$

where $\hat{J}_i$ and $\hat{K}_i$ are orbital Coulomb and exchange operators, respectively, and the a_i^γ/b_i^γ coefficients are given in Table I for all excitations considered here.

Equations (1) are solved variationally in the form

$$\langle \tilde{\phi}_i^\gamma | \, h_\gamma \, | \tilde{\phi}_j^\gamma \rangle = \delta_{ij} \tilde{\epsilon}_i^\gamma \ , \tag{2a}$$

$$\langle \tilde{\phi}_i^\gamma | \, \tilde{\phi}_j^\gamma \rangle = \delta_{ij}, \quad i, j = 1, 2, \ldots, N \tag{2b}$$

subject to orthogonality to the occupied canonical HF orbitals, employing the basis sets shown in

TABLE I. Static-exchange potentials and multiplicity factors in carbon dioxide.[a]

γ	$i=\sigma_g$	σ_u	π_u^x	π_u^y	π_g^x	π_g^y	g_γ[b]
$\sigma_g \to k\sigma_u$	$\frac{1}{2}/-1$	1/1	1/1	1/1	1/1	1/1	2
$\sigma_g \to k\pi_u$	$\frac{1}{2}/-1$	1/1	1/1	1/1	1/1	1/1	4
$\sigma_u \to k\sigma_g$	1/1	$\frac{1}{2}/-1$	1/1	1/1	1/1	1/1	2
$\sigma_u \to k\pi_g$	1/1	$\frac{1}{2}/-1$	1/1	1/1	1/1	1/1	4
$\pi_u^x \to k\sigma_g$	1/1	1/1	$\frac{1}{2}/-1$	1/1	1/1	1/1	4
$\pi_u^x \to k\pi_g^x$	1/1	1/1	$\frac{1}{4}/-3$	$\frac{5}{4}/5$	1/1	1/1	4
$\pi_u^x \to k\delta_g^{xy}$	1/1	1/1	$\frac{3}{4}/1$	1/1	1/1	1/1	8
$\pi_g^x \to k\sigma_u$	1/1	1/1	1/1	1/1	$\frac{1}{2}/-1$	1/1	4
$\pi_g^x \to k\pi_u^x$	1/1	1/1	1/1	1/1	$\frac{1}{4}/-3$	$\frac{5}{4}/5$	4
$\pi_g^x \to k\delta_u^{xy}$	1/1	1/1	1/1	1/1	$\frac{3}{4}/1$	1/1	8

[a] Values of the coefficients a_i^γ/b_i^γ appearing in the static-exchange potentials of Eq. (1). A previously reported table of coefficients (Ref. 60) contains typographical errors corrected here. We thank R. M. Pitzer for bringing these to our attention.

[b] Oscillator-strength multiplicity factors of Eq. (3).

Table II. The latter are chosen to supplement the $(10s, 5p)/[3s, 2p]$ valence basis with sufficient numbers of compact and diffuse functions to span both intravalence and Rydberg transitions in CO_2. Possible limitations of the basis of Table II are discussed below at appropriate points in the text. The pseudoenergies $\tilde{\epsilon}_i^\gamma$ and eigenfunctions $\tilde{\phi}_i^\gamma$ are used in construction of many-electron transition frequencies and oscillator strengths of the form

$$\tilde{E}_i^\gamma = \tilde{\epsilon}_i^\gamma + \epsilon_\gamma , \tag{3a}$$

$$\tilde{F}_i^\gamma = g_\gamma(\tfrac{2}{3})\tilde{E}_i^\gamma |\langle \tilde{\phi}_i^\gamma | \mu | \phi_\gamma \rangle|^2 , \tag{3b}$$

where ϵ_γ are experimental or Koopmans ionization thresholds, ϕ_γ are the canonical Hartree-Fock orbitals, and the multiplicity factors g_γ are given in Table I. The combined valence and supplemental basis sets give static-exchange excitation spectra [Eqs. (1) to (3)] of dimensionalities (N) indicated in Table II. Once a pseudospectrum of sufficient size is constructed, it is possible to turn to the question of extracting from it a reliable approximation to the underlying photoionization cross section.

In Table III is shown a typical pseudospectrum

TABLE II. Supplemental Gaussian basis functions used in CO_2 static-exchange calculations.[a]

Location	Type	Number	Exponent range[b]
	$\sigma_g(24)/\sigma_u(24)$[c]		
C/C	$s/$	12/	1.5 to 0.0008/
C/C	$/p_z$	/12	/1.5 to 0.0008
O_1 and O_2/O_1 and O_2	s/s	4/4	2.0 to 0.1/2.0 to 0.1
O_1 and O_2/O_1 and O_2	p_z/p_z	4/4	2.0 to 0.1/2.0 to 0.1
	$\pi_g(21)/\pi_u(23)$		
C/C	d_{xz}/p_x	12/12	1.5 to 0.0008/1.5 to 0.0008
O_1 and O_2/O_1 and O_2	p_x/p_x	4/4	2.0 to 0.1/2.0 to 0.1
O_1 and O_2/O_1 and O_2	d_{xz}/d_{xz}	4/4	1.0 to 0.125/1.0 to 0.125
	$\delta_g(22)/\delta_u(16)$		
C/C	$d_{xy}/$	16/	1.0 to 0.0007/
O_1 and O_2/O_1 and O_2	d_{xy}/d_{xy}	6/16	2.0 to 0.141/2.0 to 0.0007

[a] Supplement basis functions employed, in addition to the $(10s, 5p)/[3s, 2p]$ valence basis (Ref. 71), in solution of the static-exchange equations [Eqs. (1) to (3)].

[b] A geometric series variation is employed in the indicated exponent range.

[c] Numbers in parentheses refer to dimensionalities of virtual-orbital spectra [Eqs. (1) to (3)] obtained from the indicated basis sets.

TABLE III. Variationally determined static-exchange and moment-theory spectra for $1\pi_u \rightarrow k\delta_g$ excitation and ionization in CO_2.

Variational spectrum[a] Energy (eV)/f number	Moment-theory spectra[b] $n=5$	$n=10$	Energy (eV)/f number $n=15$	$n=20$
16.0138/0.038 52	16.5381/0.113 76	16.0312/0.042 17	16.0140/0.038 57	16.0138/0.038 52
16.7112/0.020 67	20.5912/0.356 05	17.1768/0.070 20	16.7529/0.927 45	16.7120/0.020 90
17.0347/0.011 31	30.0417/0.459 40	18.9848/0.135 50	17.4315/0.042 36	17.0792/0.017 02
17.2099/0.006 89	56.0764/0.325 00	21.8161/0.197 12	18.2853/0.049 48	17.4677/0.024 10
17.3232/0.006 05	158.7983/0.112 47	26.3333/0.262 07	19.3216/0.085 85	18.0639/0.045 66
17.5295/0.017 98		35.5869/0.260 71	21.4470/0.168 75	19.2155/0.094 72
18.0690/0.044 82		49.5232/0.172 75	25.5513/0.257 32	21.4174/0.170 26
19.2158/0.094 68		77.1826/0.130 53	32.8723/0.195 02	25.0628/0.001 63
21.4175/0.170 26		135.7552/0.073 57	39.9930/0.104 41	25.4841/0.241 19
25.4790/0.242 03		287.8483/0.022 07	45.0790/0.116 24	26.7161/0.017 60
26.6929/0.018 37			64.1783/0.125 67	32.9945/0.199 50
32.9942/0.199 50			73.1460/0.019 64	41.1840/0.144 07
41.1820/0.143 97			107.6701/0.090 20	46.6879/0.073 11
46.6809/0.073 19			189.5314/0.033 75	64.6604/0.125 31
64.6182/0.132 60			326.3001/0.011 98	71.3714/0.016 05
70.9125/0.017 69				107.0437/0.088 58
106.5943/0.080 48				121.5585/0.002 81
113.4874/0.010 90				189.5162/0.033 61
187.5923/0.023 98				208.1019/0.000 19
194.1148/0.009 80				326.6164/0.011 84
325.7069/0.011 42				
337.9703/0.000 55				

[a] Values obtained from Eqs. (1) to (3) employing the basis set of Table II for δ_g final state symmetry.
[b] Values obtained from Eq. (4) for the indicated values of n.

$\{\tilde{E}_i^\gamma, \tilde{F}_i^\gamma;\ i=1,2,\ldots,22\}$ obtained from the development of Eqs. (1) to (3) using the appropriate basis set of Table II, corresponding in this case to $1\pi_u \rightarrow n\delta_g$ transitions in CO_2. It is seen that the first six transition energies accumulate at the ionization threshold (~17.7 eV), and that the corresponding f numbers decrease smoothly until the threshold is reached. The variationally determined [Eq. (2)] energies and strengths of Table III are evidently highly irregular above the ionization threshold, and do not seem to vary smoothly in any way, suggesting that perhaps there is little, if any, information in the pseudospectrum pertaining to the underlying photoionization profile. However, also shown in Table III are spectra of energies ϵ_i and strengths f_i that satisfy the moment equations[69,70]

$$\sum_{i=1}^{22} \tilde{F}_i^\gamma (\tilde{E}_i^\gamma)^{-k} \equiv \tilde{\mu}_k = \sum_{i=1}^{n} f_i \epsilon_i^{-k}, \quad k=0,1,\ldots,2n-1 \tag{4}$$

for $n=5$, 10, 15, and 20. The ϵ_i and f_i are seen to vary smoothly with the index i for $n \leq 10$, suggesting that such point spectra can perhaps be employed in constructing reliable approximation to the underlying photoionization continuum. By contrast, the spectrum for $n=15$ is somewhat irregular, and for $n=20$ the original static-exchange pseudospectrum $\tilde{E}_i^\gamma, \tilde{F}_i^\gamma$ is almost recovered from Eq. (4).

The moment-theory spectra ϵ_i and f_i of Eq. (4) are central to the Stieltjes-Tchebycheff approach to molecular photoionization calculations in Hilbert space.[69,70] They are the generalized Gaussian quadratures of the (unknown) photoexcitation/ionization cross section, provided that the spectral moments employed in their construction [Eq. (4)] are reliable approximations to the correct static-exchange values. When this is the case, a situation that can be assured by making the basis set sufficiently large and n sufficiently small, the ϵ_i, f_i can be used in constructing photoionization cross sections in a variety of ways described in detail elsewhere.[69,70] It is sufficient to note here that the moment-theory pseudospectra [Eq. (4)] provide bounds on the cumulative oscillator-strength distribution, and, consequently, are appropriate for smoothing techniques. By contrast, the original pseudospectrum $\tilde{E}_i^\gamma, \tilde{F}_i^\gamma$ does not provide bounds and is generally so irregular that it is not possible to extract a reliable cross section from it directly.[73] Solutions of Eq. (4) for the ϵ_i, f_i when the $\tilde{E}_i^\gamma, \tilde{F}_i^\gamma$ are given are obtained from a series of highly stable algorithms that do not involve explicit computations of the moments $\tilde{\mu}_k$.[75] It is

nevertheless convenient to view the ϵ_i, f_i in the context of Eq. (4), since these ensure that the important bounding theorem indicated above is satisfied.[76] The interested reader is referred to the literature for detailed descriptions of the moment approach to molecular photoionization studies.[69,70]

In the present calculations, the basis sets of Table II are found to give pseudospectra that provide reliable Gaussian quadrature points and weights [Eq. (4)] for $n \lesssim 10$–12. The cumulative oscillator-strength distributions obtained from these for $5 \lesssim n \lesssim 12$ are fit with polynomials in $1/\epsilon$ and the results differentiated to obtain corresponding densities. The resulting partial-channel cross sections are found to be smooth and generally stable to small variations in the basis sets, suggesting that reliable approximations to the correct static-exchange results are obtained.

III. PHOTOEXCITATION AND IONIZATION IN CO_2

Qualitative descriptions of the nine occupied canonical Hartree-Fock molecular orbitals in CO_2 provide a basis for clarifying the static-exchange spectra obtained from the present calculations.[42-45] The outermost $1\pi_g$ (n) orbital is nonbonding and comprised primarily of oxygen atom $2p$ orbitals, whereas $1\pi_u$ (π) is strongly C–O π bonding, comprised of carbon and oxygen $2p$ orbitals. The $3\sigma_u$ (σ) and $4\sigma_g$ (σ) molecular orbitals in CO_2 are nonbonding to weakly C–O bonding σ orbitals comprised of carbon and oxygen $2s$-$2p$ hybrids, whereas the inner-valence-shell $2\sigma_u$ (σ) and $3\sigma_g$ (σ) orbitals are similarly comprised but are strongly C–O σ bonding. It is perhaps also helpful to note that the $3\sigma_g$, $2\sigma_u$, $4\sigma_g$, and $3\sigma_u$ molecular orbitals have nodal structures that resemble approximately those of the eigenfunctions of a particle in a one-dimensional box.[77] Finally, the $2\sigma_g$(C1s), $1\sigma_u$ (O1s), and $1\sigma_g$ (O1s) orbitals correspond approximately to carbon $1s$ orbitals and appropriate symmetry combinations of oxygen $1s$ orbitals. There are semiquantitative similarities between certain of the occupied orbitals in CO_2 and those in CO, the spectrum of which has been previously studied in considerable detail.[59] The approximate correspondences $1\pi_u$ $(\pi) \sim 1\pi$; $3\sigma_u$ $(\sigma) \sim 5\sigma$; $4\sigma_g$ $(\sigma) \sim 4\sigma$; $2\sigma_u$, $3\sigma_g \sim 3\sigma$; $2\sigma_g$ (C1s) $\sim 2\sigma$; $1\sigma_u$ (O1s), $1\sigma_g$ (O1s) $\sim 1\sigma$ will aid in the interpretation of the discrete and continuum spectrum in CO_2.

The unoccupied virtual valence orbitals in CO_2 can be characterized qualitatively as $2\pi_u$ (π^*), $5\sigma_g$ (σ^*), and $4\sigma_u$ (σ^*), and the approximate correspondences $2\pi_u(\pi^*) \sim 2\pi(\pi^*)$; $5\sigma_g$ (σ^*), $4\sigma_u$ (σ^*) $\sim 6\sigma$ (σ^*) with virtual orbitals in CO can be made. Moreover, their nodal structures are also similar to those of the higher-lying eigenfunctions of a particle in a one-dimensional box.[77] Of course, these designations for the virtual valence orbitals in CO_2 are only approximate, and the correct functions are combinations of all the compact and diffuse functions employed in the calculations (Table II). Nevertheless, when discussing the calculated static-exchange spectra it is convenient to retain approximate designations in order to distinguish between strong intravalence transitions and weaker Rydberg-like transitions involving the more diffuse basis functions of Table II. It can be anticipated that the $2\pi_u$ (π^*) orbital in CO_2 will contribute primarily to the discrete excitation series, whereas the $4\sigma_u$ (σ^*) and $5\sigma_g$ (σ^*) orbitals will be higher lying, and presumably will appear as diabatic states in the various photoionization continua.[57-69] Consequently, a significant number of $\sigma \rightarrow \sigma^*$ resonancelike features are expected in the partial-channel photoionization cross sections in CO_2.

It is convenient in the following to discuss separately the outer-valence-shell, inner-valence-shell, and K-edge absorption cross sections in CO_2.

A. Outer-valence-shell cross sections

A semiquantitative description of the outer-valence-shell $1\pi_g$ (n), $1\pi_u$ (π), $3\sigma_u(\sigma)$, and $4\sigma_g$ (σ) excitation spectra is given in Fig. 1 in compari-

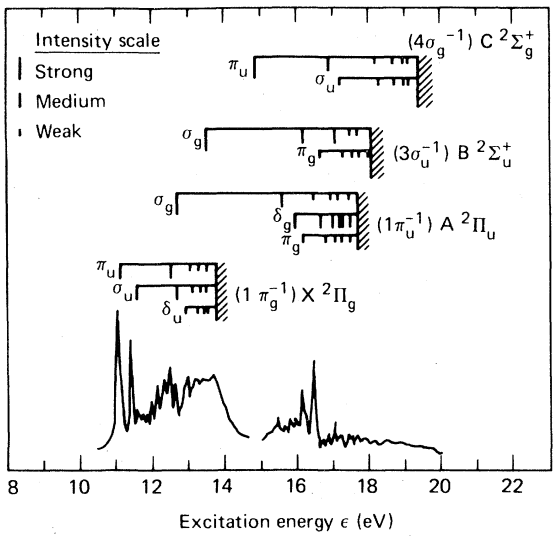

FIG. 1. Static-exchange outer-valence-shell discrete excitation spectra in CO_2 obtained from Eqs. (1) to (3) employing the basis sets of Sec. II and Table II. Numerical values are given in Tables IV to VI. The experimental data is a 150 eV electron-impact-excitation spectrum (Ref. 18). Intensity scale: strong, $f > 0.1$; medium, $0.1 > f > 0.01$; weak, $0.01 > f$.

TABLE IV. $1\pi_g$ excitation spectra in CO_2 (I.P. = 13.8 eV).

Present results[a] Energy (eV)/f number	Experimental results[b] Energy (eV)/intensity	Defect estimates[c] Energy (eV)/f number
	$(1\pi_g)\,^1\Sigma_g^+ \rightarrow (np\sigma_u)\,^1\Pi_u$	
11.61/0.029 9	11.05/strong	11.21/0.062 6
12.70/0.012 8	12.48/	12.53/0.021 2
13.14/0.006 5	13.03/	13.04/0.009 6
13.36/0.003 7		13.30/0.005 1
13.55/		13.44/0.003 0
	$(1\pi_g)\,^1\Sigma_g^+ \rightarrow (np\pi_u)\,^1\Sigma_u^+$	
11.15/0.046 0	11.38/strong	11.21/0.029 1
12.55/0.011 8	12.64/	12.53/0.009 8
13.07/0.004 9	13.11/	13.04/0.004 4
13.32/0.002 5		13.30/0.002 4
13.48/		13.44/0.001 4
	$(1\pi_g)\,^1\Sigma_g^+ \rightarrow (nf\delta_u)\,^1\Pi_u$	
12.95/0.001 01	12.97/allowed	12.93/0.004 68
13.26/0.000 86	13.27/	13.24/0.002 39
13.45/0.000 79		13.40/0.001 39
13.57/		13.50/0.000 87

[a] Values obtained from the development of Eqs. (1) to (3) employing the basis sets of Sec. II and Table II. The series are made to converge on the experimental adiabatic threshold of 13.8 eV (Ref. 21).

[b] Taken from the analysis and compilations of C. Fridh, L. Åsbrink, and E. Lindholm, Chem. Phys. 27, 169 (1978). The $1\pi_g \rightarrow 2\pi_u$ intravalence transition not included in the present calculations is assigned by these authors at ~12.5 eV.

[c] Positions obtained from the Rydberg formula $[\epsilon_n = \epsilon_t - 13.6/(n-\delta)^2]$ and f numbers from the Coulomb approximation $[f_n = g(\epsilon_t)/(n-\delta)^3]$ using quantum defects of $\delta = 0.7$, 0.7, and 0.0 for $np\sigma_u$, $np\pi_u$, and $nf\delta_u$ series, respectively, and the oscillator-strength densities at threshold $[g(\epsilon_t)$ a.u.] of Fig. 2. The n values are $n = 3, 4, \ldots$, for the $np\sigma_u$ and $np\pi_u$ series, whereas the $nf\delta_u$ series begins with an n value of 4, as is discussed further in the text.

son with a measured electron impact-excitation profile.[18] Numerical values of the calculated transition frequencies and f numbers are given in Tables IV to VI, along with experimental assignments and quantum-defect estimates.[51,52] The corresponding partial-channel photoionization cross sections are reported and compared with $(e,2e)$, line-source, fluorescence, and synchrotron radiation measurements in Figs. 2 to 6.[30-41] The calculated results shown in these tables and figures are generally stable to basis set variations and, consequently, should provide excellent approximations to the correct separated-channel static-exchange values, as indicated in the preceding section.

1. $1\pi_g(n)$ (I.P. = 13.8 eV)

The $1\pi_g \rightarrow n\sigma_u$ excitations of Fig. 1 and Table IV evidently form an $np\sigma_u$ Rydberg series of moderate intensity in general accord with experimental assignments and quantum-defect estimates using $\delta = 0.7$ (Refs. 51 and 52). Although theoretical studies of intravalence transitions in CO_2 involving $1\pi_g$ excitation have been reported,[46-50] there are apparently no previous studies of the Rydberg excitations available for comparison with the present results. The $1\pi_g \rightarrow k\sigma_u$ cross section of Fig. 2(a) evidently exhibits a maximum at ~20 eV. This feature can be assigned as a diabatic $1\pi_g \rightarrow 4\sigma_u$ (σ^*) or $n \rightarrow \sigma^*$ intravalence transition in the $1\pi_g \rightarrow k\sigma_u$ cross section, confirming the appearance of the $4\sigma_u$ (σ^*) virtual orbital in the photoionization continuum.

The $1\pi_g \rightarrow n\pi_u$ excitations in CO_2 are expected to include a strong $1\pi_g \rightarrow 2\pi_u$ (π^*) or $n \rightarrow \pi^*$ transition.[18,51,52] Consequently, in order to obtain a meaningful theoretical excitation spectrum in the presence of this strong feature, which can spuriously perturb the photoabsorption and ionization spectrum, a triplet-coupled static-exchange calculation is performed in this case.[63] In this way the $2\pi_u$ (π^*) orbital is lowered significantly in energy relative to the singlet-coupled result, whereas the Rydberg states and continuum spectrum are

TABLE V. $1\pi_u$ excitation spectra in CO_2 (I.P. = 17.7 eV).

Present results[a] Energy (eV)/f number	Experimental values[b] Energy (eV)/intensity	Defect estimates[c] Energy (eV)/f number
	$(1\pi_u)\ ^1\Sigma_g^+ \rightarrow (ns\sigma_g)\ ^1\Pi_u$	
12.73/0.357 1	~13.5/strong	
15.57/0.041 2	15.76/	14.32/0.025 5
16.52/0.009 8	16.45/	16.20/0.007 6
16.94/0.003 6		16.87/0.003 2
17.16/0.001 7		17.18/0.001 6
17.45/		17.34/0.000 9
	$(1\pi_u)\ ^1\Sigma_g^+ \rightarrow (nd\pi_g)\ ^1\Sigma_u^+$	
16.18/0.000 517	15.80/weak	16.20/0.001 01
16.80/0.000 243	16.46/	16.87/0.000 43
17.08/0.000 129		17.18/0.000 22
17.24/0.000 083		17.34/0.000 13
17.49/		17.44/0.000 08
	$(1\pi_u)\ ^1\Sigma_g^+ \rightarrow (nd\delta_g)\ ^1\Pi_u$	
16.01/0.077 0		16.20/0.111
16.71/0.041 4		16.87/0.035
17.03/0.022 6		17.18/0.024
17.21/0.013 8		17.34/0.013
17.32/0.012 1		17.44/0.009
17.53/		17.51/0.006

[a] As in Table IV, employing the experimental adiabatic photoionization threshold of 17.7 eV (Ref. 21).

[b] As in Table IV.

[c] As in Table IV, employing quantum defects of $\delta = 1.0$, 0.0, and 0.0 for $ns\sigma_g$, $nd\pi_g$, and $nd\delta_g$ series, respectively, for $n = 3, 4, \ldots$, and the oscillator-strength densities at threshold of Fig. 3(a).

left largely unperturbed. The resulting discrete excitations of Fig. 1 and Table IV are seen to be in general accord with the assigned $np\pi_u$ Rydberg series,[52] and the corresponding $1\pi_g \rightarrow k\pi_u$ continuum of Fig. 2(a) is appropriately weak. Introduction of the Rydberg-valence interaction is expected to change the positions and strengths of the discrete excitations somewhat, but should leave the $1\pi_g \rightarrow k\pi_u$ continuum largely unperturbed. Referring to Fig. 1, it is evident that somewhat better agreement with the experimental positions obtains if the $1\pi_g \rightarrow n\sigma_u$ and $1\pi_g \rightarrow n\pi_u$ assignments are interchanged.[51,52]

Finally, the $1\pi_g \rightarrow n\delta_u$ series of Fig. 1 and Table IV is seen to be in good accord with the assigned $nf\delta_u$ Rydberg transitions.[51,52] It is important to note that this series apparently begins with a principle quantum of $n = 4$, rather than $n = 3$. The corresponding $1\pi_g \rightarrow k\delta_u$ continuum of Fig. 2(a) is seen to contain a strong maximum that can be given a $2p \rightarrow kd$ designation, and arises from the more compact portions of the δ_u basis set, in accord with the absence of an $n = 3$ transition in the discrete spectrum.

The three $1\pi_g$ photoionization components of Fig. 2(a) are qualitatively similar to $1\pi_g \rightarrow k\sigma_u$, $k\pi_u$, and $k\delta_u$ profiles in F_2 and O_2.[60-62] Moreover, the $1\pi_g \rightarrow k\delta_u$ component resembles a $2p \rightarrow kd$ atomic-like cross section, with which it presumably correlates in the separated-atom limit. With the exception of the $1\pi_g \rightarrow 4\sigma_u$ (σ^*) resonance contribution at ~20 eV, the $1\pi_g \rightarrow k\sigma_u$ component is similar to a $2p \rightarrow ks$ atomic cross section, and the $1\pi_u \rightarrow k\pi_g$ component is presumably weak as a consequence of its correlation with the dipole forbidden $2p \rightarrow kp$ continuum in the separated-atom limit. Evidently, the nonbonding nature of the $1\pi_g$ orbital in CO_2 results in considerable atomic oxygen $2p$-like character in its photoionization cross section.

The three components of Fig. 2(a) are combined in Fig. 2(b), where the calculated vertical electronic $(1\pi_g^{-1})X\ ^2\Pi_g$ partial-channel cross section is compared with the results of $(e, 2e)$,[30] synchrotron-radiation[33] and line-source[38-41] measurements. The experimental data correspond to integration of the measured photoelectron spectra over vibrational and rotational substructures, and so comparison with vertical ionization cal-

TABLE VI. $3\sigma_u$ (I.P. = 18.1 eV) and $4\sigma_g$ (I.P. = 19.4 eV) excitation spectra in CO_2.

Present results[a] Energy (eV)/f number	Experimental values[b] Energy (eV)/intensity	Defect estimates[c] Energy (eV)/f number
	$(3\sigma_u)\,^1\Sigma_g^+ \rightarrow (ns\sigma_g)\,^1\Sigma_u^+$	
13.56/0.168 7	13.04/strong	13.37/0.349 0
16.22/0.035 5	16.22/	16.21/0.087 1
17.10/0.014 1	17.07/	17.09/0.033 9
17.48/0.007 2		17.46/0.016 5
17.68/0.004 8		17.66/0.009 3
18.05/		17.78/0.005 7
	$(3\sigma_u)\,^1\Sigma_g^+ \rightarrow (nd\pi_g)\,^1\Pi_u$	
16.65/0.006 01	16.49/strong	16.57/0.009 07
17.28/0.003 01	17.29/	17.23/0.003 83
17.57/0.001 64	17.54/	17.54/0.001 96
17.73/0.001 05		17.70/0.001 13
17.97/		17.80/0.000 71
	$(4\sigma_g)\,^1\Sigma_g^+ \rightarrow (np\sigma_u)\,^1\Sigma_u^+$	
17.23/0.002 73		16.83/0.020 1
18.31/0.000 69	18.16/weak	18.15/0.006 8
18.74/0.000 26	18.67/	18.66/0.003 1
18.96/0.000 12		18.92/0.001 7
19.16/		19.06/0.001 0
	$(4\sigma_g)\,^1\Sigma_g^+ \rightarrow (np\pi_u)\,^1\Pi_u$	
14.87/0.461 8	15.5/0.25	
16.90/0.014 6		16.83/0.007 8
18.19/0.003 3	18.26/weak	18.15/0.002 7
18.69/0.001 3	18.85/	18.66/0.001 2
18.93/0.000 7		18.92/0.000 6
19.10/		19.06/0.000 4

[a] As in Table IV, employing the indicated experimental adiabatic ionization thresholds (Ref. 21).

[b] As in Table IV. The $4\sigma_g \rightarrow 2p\pi_u$ energy and f number are from Ref. 46.

[c] As in Table IV, employing quantum defects of 1.3, 0.7, and 0.0 for ns, np, and nd series, respectively, for $n = 3, 4, \ldots$, and the threshold oscillator-strength values of Figs. 4. and 6.

culations is expected to be generally appropriate. Evidently, the static-exchange calculations are in excellent quantitative agreement with the measured data above ~30 eV, although there is an apparent discrepancy at lower energy. The effects of intensity borrowing,[54, 55, 68] also shown in the figure, reduce the discrepancy somewhat, but apparently do not eliminate it entirely. This discrepancy will be tentatively attributed in the following subsection to coupling with scattering states in the $(1\pi_u^{-1})A\,^2\Pi_u$ channel that is neglected in the present calculations.

2. $1\pi_u$ (π) spectra (I.P. = 17.7 eV)

The calculated $1\pi_u \rightarrow n\sigma_g$ excitations of Fig. 1 and Table V are evidently in general agreement with the assigned $ns\sigma_g$ Rydberg series, and with the quantum-defect estimates obtained using the value $\delta = 1.0$. Since the resonance in the $1\pi_u \rightarrow ns\sigma_g$ series is particularly strong, it is regarded here as primarily intravalence $[1\pi_u \rightarrow 5\sigma_g\ (\sigma^*)]$ in character, with the second term in the series corresponding to an $n = 3$ principle quantum number. When this view is adopted, which is not in accord with the recent spectral analysis,[51, 52] the higher members of the series are in excellent agreement with the quantum-defect estimates, although the lower members exhibit some intravalence perturbation. Moreover, the $1\pi_u \rightarrow 5\sigma_g\ (\sigma^*)$ intravalence transition may account, in part, for the continuumlike behavior in the 150 eV electron impact-excitation spectrum in the 13 to 14 eV interval associated with photoproduction of CO in the $A\,^1\Pi$ state.[18] Because the discrete transitions are strong in this case, the $1\pi_u \rightarrow k\sigma_g$ photoionization cross section of Fig. 3(a) is correspondingly

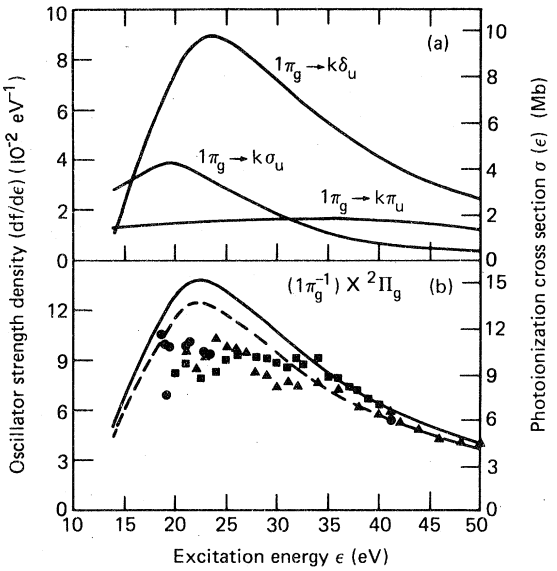

FIG. 2. (a) Static-exchange cross sections in CO_2 for $1\pi_g \rightarrow k\sigma_u$, $k\pi_u$, and $k\delta_u$ photoionization, obtained from the Stieltjes-Tchebycheff development of Eqs. (1) to (4) and the basis sets of Table II; (b) partial-channel photoionization cross sections for production of $(1\pi_g^{-1})X\ ^2\Pi_g$ CO_2^+ parent ions; (——), vertical-electronic static-exchange results obtained from Fig. 1(a); (---), static-exchange results including intensity-borrowing effects (Refs. 53, 54, and 58); ▲, $(e,2e)$ data (Ref. 30); ■, synchrotron radiation data (Ref. 33); ●, line-source data (Refs. 38–41). σ(Mb) = 109.75$df/d\epsilon$ (eV^{-1}); 1 Mb = 10^{-18} cm^2.

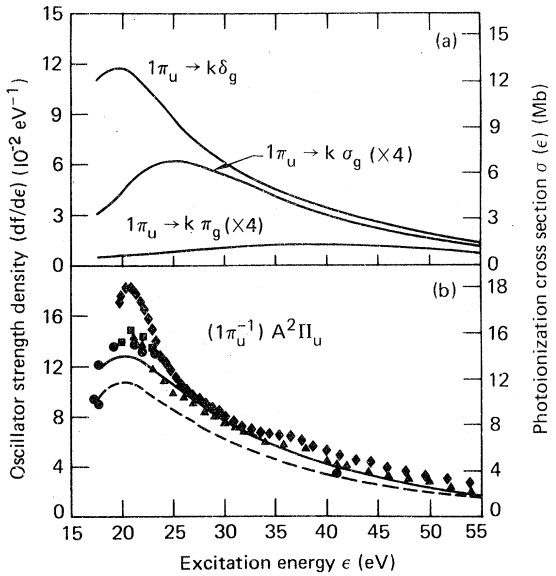

FIG. 3. (a) As in Fig. 2(a) for $1\pi_u \rightarrow k\sigma_g$, $k\pi_g$, and $k\delta_g$ photoionization; (b) as in Fig. 2(b) for production of $(1\pi_u^{-1})A\ ^2\Pi_u$ parent ions; the $(e,2e)$ (▲) and synchrotron radiation (■) data are constructed from the measure sum of $A\ ^2\Pi_u$ and $B\ ^2\Sigma_u^+$ channel cross sections as discussed in the text; ♦, fluorescence cross section (Ref. 37).

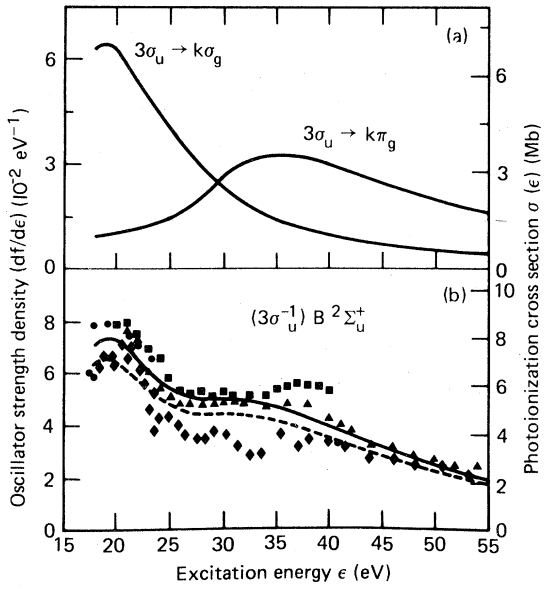

FIG. 4. (a) As in Fig. 2(a) for $3\sigma_u \rightarrow k\sigma_g$ and $k\pi_g$ photoionization; (b) as in Fig. 3(b) for production of $(3\sigma_u^{-1})B\ ^2\Sigma_u^+$ parent ions; fluorescence cross section taken from Ref. 36.

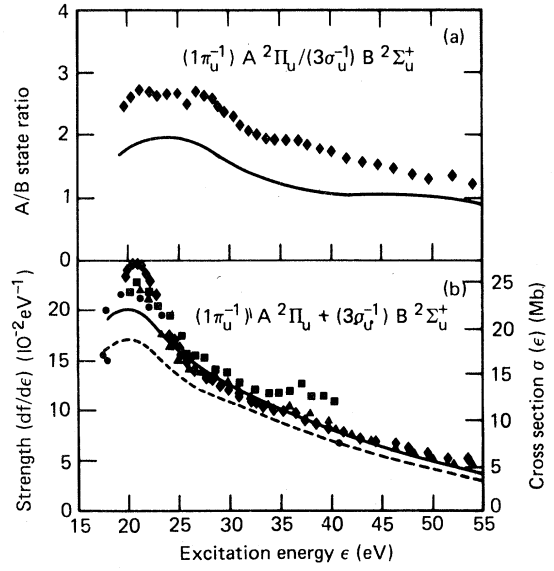

FIG. 5. (a) Ratio of $(1\pi_u^{-1})A\ ^2\Pi_u$ and $(3\sigma_u^{-1})B\ ^2\Sigma_u^+$ partial-channel photoionization cross sections in CO_2; (——), vertical-electronic static-exchange calculations obtained from Figs. (3) and (4); ♦, fluorescence data obtained from Figs. (3) and (4). Additional measurements of fluorescence cross sections at 21.2 eV give $A/B \cong 2.2$–1.5 (Refs. 78–81), whereas high-resolution PES studies (Ref. 40) give ~0.65 at this energy; (b) sum of $(1\pi_u^{-1})A\ ^2\Pi_u$ and $(3\sigma_u^{-1})B\ ^2\Sigma_u^+$ partial-channel photoionization cross sections in CO_2; (——) and (----), vertical-electronic static-exchange results from Figs. (3) and (4); ♦, fluorescence data from Figs. (3) and (4); ▲, $(e,2e)$ data (Ref. 30); ■, synchrotron radiation data (Ref. 33); ●, line-source data (Refs. 38–41).

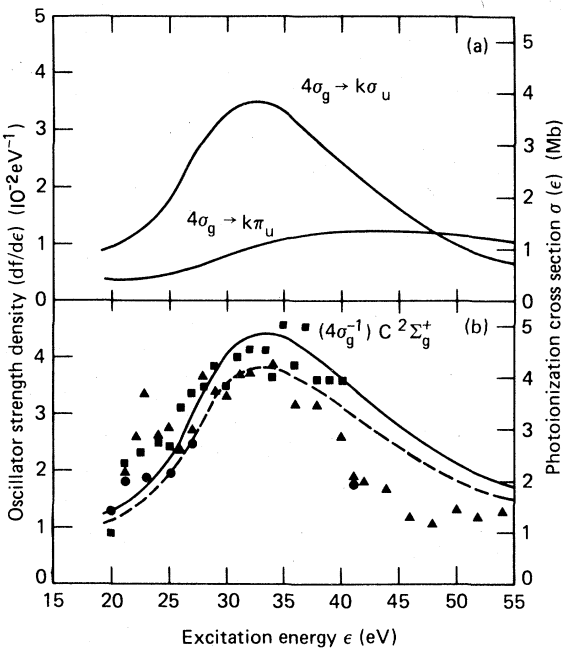

FIG. 6. (a) As in Fig. 2(a) for $4\sigma_g \rightarrow k\sigma_u$ and $k\pi_u$ photoionization; (b) as in Fig. 2(b) for production of $(4\sigma_g^{-1})C\ ^2\Sigma_g^+$ parent ions in CO_2.

weak.

The $1\pi_u \rightarrow k\pi_g$ series of Fig. 1 and Table V is evidently very weak, in accord with the spectral assignment,[52] and the corresponding $1\pi_u \rightarrow k\pi_g$ profile of Fig. 3(a) is broad and flat, extending to high energy.

Finally, the calculated $1\pi_u \rightarrow n\delta_g$ series of Table V is evidently in good accord with the $nd\delta_g$ quantum-defect estimates, although experimental assignments are apparently not available at present. The corresponding $1\pi_u \rightarrow k\delta_g$ cross section shown in Fig. 3(a) is very strong and has a distinct $2p \rightarrow kd$ atomiclike maximum at ~20 eV.

The three $1\pi_u$ photoionization components of Fig. 3(a) are qualitatively similar to corresponding $1\pi_u \rightarrow k\sigma_g$, $k\pi_g$, and $k\delta_g$ profiles in O_2.[61,62] As in the case of O_2, the $1\pi_u \rightarrow k\delta_g$ component in CO_2 is largely $2p \rightarrow kd$ atomiclike in nature, and the $1\pi_u \rightarrow k\sigma_g$ and $k\pi_g$ components resemble $2p \rightarrow ks$ and kp atomic-like cross sections, respectively.

The three $1\pi_u$ contributions are combined and compared with experiment in Fig. 3(b). Evidently, with the exception of the 20–25 eV energy interval, the calculated results are in excellent agreement with the partial-channel cross section obtained from fluorescence measurements.[37] Since the $(e, 2e)$ and tunable-source PES (photoelectron spectroscopy) studies do not separate the $A\ ^2\Pi_u$ and $B\ ^2\Sigma_u^+$ channels, the data of Fig. 3(b) in these cases are obtained by employing the theoretically determined $A\ ^2\Pi_u/B\ ^2\Sigma_u^+$ ratio in conjunction with the measured sum of the A and B state contributions.[30,33,38–41] It is seen that the calculated vertical electronic $(1\pi_u^{-1})A\ ^2\Pi_u$ partial-channel cross section is in excellent agreement with the data points obtained in this manner. All four experimental results evidently provide support for the strong $2p \rightarrow kd$ atomiclike feature in the $1\pi_u \rightarrow k\delta_g$ profile near threshold. The effects of intensity borrowing also shown in Fig. 3(b) may be partially offset by vibrational averaging not included in the present study.

It is of some interest to hypothesize that the discrepancy between the theoretical results and the fluorescence data in the ~20–25 eV interval is due to coupling with the $(1\pi_g^{-1})X\ ^2\Pi_g$ channel. Specifically, the oxygen-atom $2p$ character of the $1\pi_g$ and $1\pi_u$ orbitals suggests that $1\pi_g^{-1}k\delta_u$ and $1\pi_u^{-1}k\delta_g$ configurations have significant spatial overlap and can mix, causing coupling in the $k\delta_u$ and $k\delta_g$ scattering states, and possibly shifting intensity from the $1\pi_g^{-1}$ to the $1\pi_u^{-1}$ channel. A similar situation also obtains in the case of the $1\pi_g^{-1}$ and $1\pi_u^{-1}$ channels in O_2.[61,62] It should be noted, however, that high-resolution PES measurements of the $A\ ^2\Pi_u/B\ ^2\Sigma_u^+$ ratio at 21.2 eV (Ref. 40) do not support the CO_2^+ fluorescence data in this energy interval, as is discussed somewhat further below.

3. $3\sigma_u$ (σ) spectra (I.P. = 18.1 eV)

In Fig. 1 and Table VI the calculated $3\sigma_u \rightarrow n\sigma_g$ discrete excitations are seen to be in excellent agreement with the assigned $ns\sigma_g$ Rydberg series, which has the rather large defect of 1.3 (Ref. 52). The $5\sigma_g$ (σ^*) virtual valence orbital evidently appears just above threshold in the $3\sigma_u \rightarrow k\sigma_g$ cross section of Fig. 4(a) as a diabatic resonancelike contribution, giving rise to a prominent feature in the spectrum at ~19 eV. As opposed to the situation in the $1\pi_u \rightarrow n\sigma_g/k\sigma_g$ spectrum discussed above, in which case the $5\sigma_g$ (σ^*) orbital contributes to states primarily below threshold, in the present case its contribution is largely concentrated in the $3\sigma_u \rightarrow k\sigma_g$ continuum, although the relatively large quantum defect may indicate Rydberg-valence perturbation in this case. The presence of the low-lying $5\sigma_g$ (σ^*) virtual orbital in the CO_2 spectrum causes the $3\sigma_u \rightarrow k\sigma_g$ cross section to differ from the $5\sigma \rightarrow k\sigma$ profile in CO, which exhibits a $5\sigma \rightarrow \sigma^*$ resonance ~10 eV above threshold.[59]

The $3\sigma_u \rightarrow n\pi_g$ series of Fig. 1 and Table VI is in excellent accord with the assigned $nd\pi_g$ Rydberg series. Although the calculated intensities are weaker than the measured spectra, they are in excellent accord with the defect estimates. Evidently, the corresponding $3\sigma_u \rightarrow k\pi_g$ continuum of Fig. 4(a) includes a broad feature at 35 eV that

can be attributed to d-orbital contributions.

The two $3\sigma_u^{-1}$ photoionization components of Fig. 4(a) are combined in Fig. 4(b), where the calculated vertical electronic $(3\sigma_u^{-1})B\,^2\Sigma_u^+$ partial-channel photoionization cross section is compared with experimental values. Evidently, the theoretical results are somewhat larger than the measured fluorescence data for this channel in the ~25 to 40 eV interval,[36] although agreement is satisfactory at higher and lower energies. As in the case of the $(1\pi_u^{-1})A\,^2\Pi_u$ state, the experimental $(e,2e)$ and tunable-source PES data of Fig. 4(b) are constructed from the measured sum of the A and B channels employing the theoretically predicted A/B ratio to effect a separation. The calculated $(3\sigma_u^{-1})B\,^2\Sigma_u^+$ cross section is evidently in good agreement with the partial-channel data obtained in this manner. In addition, it is clear that the strong feature just above threshold in the experimentally determined $B\,^2\Sigma_u^+$ cross section of Figs. 4(b) can be attributed to the $5\sigma_g$ (σ^*) valence virtual orbital contribution in the $3\sigma_u \rightarrow k\sigma_g$ component of Fig. 4(a). There is also some evidence in the experimental data of the second peak in this channel due to the $3\sigma_u \rightarrow k\pi_g$ contribution.

4. $(1\pi_u^{-1})A\,^2\Pi_u$ and $(3\sigma_u^{-1})B\,^2\Sigma_u^+$ channel sum and ratio

Because the $(e,2e)$[30] and tunable-source PES[33,38-41] measurements do not resolve the $(1\pi_u^{-1})A\,^2\Pi_u$ and $(3\sigma_u^{-1})B\,^2\Sigma_u^+$ partial-channel cross sections, the theoretically determined $A\,^2\Pi_u/B\,^2\Sigma_u^+$ ratio has been used to effect a separation of the experimental data in Figs. 3 and 4. Consequently, it is of interest to make explicit comparison of the calculated $A\,^2\Pi_u/B\,^2\Sigma_u^+$ ratio with values obtained from independent fluorescence measurements of the separate $A\,^2\Pi_u$ and $B\,^2\Sigma_u^+$ cross sections,[36,37] and of the calculated sum of the A and B channel cross sections with the corresponding $(e,2e)$ and tunable-source PES data.

In Fig. 5(a) is shown the calculated static-exchange $A\,^2\Pi_u/B\,^2\Sigma_u^+$ ratio in comparison with values obtained from separate A and B state fluorescence measurements.[36,37] Evidently, the measured ratio is somewhat larger than the calculated values at all but the highest excitation energies. However, the sum of the two fluorescence cross sections is in good agreement with the calculated sum shown in Fig. 5(b), except below 25 eV excitation energy. The results of Fig. 3, 4, and 5 indicate that the measured $(1\pi_u^{-1})A\,^2\Pi_u$ fluorescence data are generally larger than the static-exchange result [Fig. 3(b)], whereas the measured $(3\sigma_u^{-1})B\,^2\Sigma_u^+$ fluorescence data are generally smaller than the static-exchange result [Fig. 4(b)]. Consequently, forming the $A\,^2\Pi_u/B\,^2\Sigma_u^+$ ratio exaggerates the discrepancy between the theoretical and experimental results in these cases [Fig. 5(a)]. By contrast, the sum of the $A\,^2\Pi_u$ and $B\,^2\Sigma_u^+$ fluorescence measurements is in good agreement with the static-exchange calculations above 25 eV, apparently as a consequence of compensation in the discrepancies in each case [Figs. 3(b) and 4(b)]. Indeed, it would seem that the major discrepancy between the fluorescence measurements and the present calculations occurs in the low-energy (~20 to 25 eV) interval, where the $A\,^2\Pi_u$ measurements are significantly larger than the calculated values [Fig. 4(b)]. It is of some interest to note in this connection that other fluorescence cross section measurements of the A/B ratio in CO_2 at 21.2 eV give values (~1.5–2.2)[78-81] significantly less than the experimental result at this energy shown in Fig. 5(a). Moreover, a high resolution PES measurement gives 0.65 for the A/B ratio at 21.2 eV,[40] and this value is apparently supported by estimates based on lower-resolution PES data.[30,33] Further refinements of the PES studies are clearly in order to help clarify the situation.[82]

Also shown in Fig. 5(b) are the $(e,2e)$ and tunable-source PES measurements of the sum of the $A\,^2\Pi_u$ and $B\,^2\Sigma_u^+$ cross sections.[30,33,38-41] These are seen to be in very good agreement with the static-exchange calculations and to verify the presence of the strong features near threshold in both $1\pi_u^{-1}$ and $3\sigma_u^{-1}$ cross sections.

5. $4\sigma_g$ (σ) spectra (I.P. = 19.4 eV)

The $4\sigma_g \rightarrow n\sigma_u$ excitations of Fig. 1 and Table VI evidently correspond to a weak $np\sigma_u$ Rydberg series, although the first member of the series has yet to be assigned. Evidently, the quantum-defect estimates of f numbers are an order of magnitude larger than the static-exchange calculations, suggesting that the oscillator-strength density of Fig. 6(a) may be an overestimate at threshold in this case. The corresponding $4\sigma_g \rightarrow k\sigma_u$ photoionization cross section of Fig. 6(a) is seen to contain a prominent maximum at ~30 eV that can be attributed to a $4\sigma_g$ (σ) $\rightarrow 4\sigma_u$ (σ^*) diabatic intravalence transition. This feature presumably corresponds to the strong lower-lying $4\sigma \rightarrow \sigma^*$ resonance in CO (Ref. 59) in view of the correspondence between 4σ and $4\sigma_g$ orbitals indicated above.

An expected strong $4\sigma_g$ (σ) $\rightarrow 2\pi_u$ (π^*) intravalence transition is evidently present in the $4\sigma_g \rightarrow n\pi_u$ series of Fig. 1 and Table VI, in general accord with the results of more elaborate calculations.[46] Although the first member of the $np\pi_u$ Rydberg series has not been assigned as yet, the calculations are in good agreement with the two other assigned states and with the quantum-defect esti-

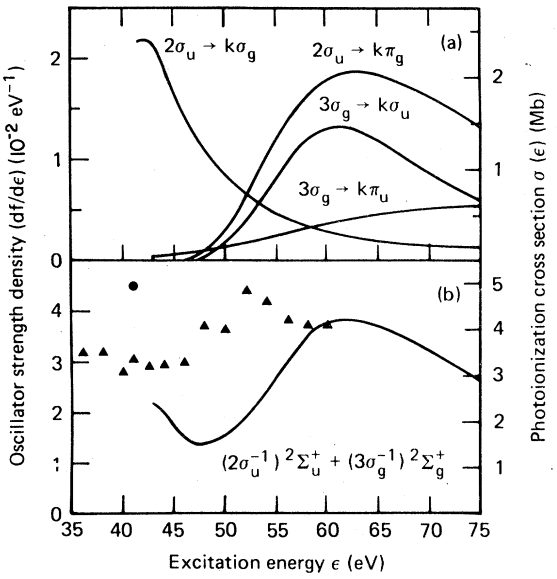

FIG. 7. (a) As in Fig. 2(a) for $2\sigma_u \rightarrow k\sigma_g$ and $k\pi_g$ and $3\sigma_g \rightarrow k\sigma_u$ and $k\pi_u$ photoionization; (b) as in Fig. 2(b) for production of inner-valence-shell many-electron parent ionic states in CO_2.

mates. Apparently, the corresponding $4\sigma_g \rightarrow k\pi_u$ cross section of Fig. 6(a) is weak and exhibits a broad maximum center at ~40 eV, presumably as a consequence of *kd* contributions.

The $(4\sigma_g^{-1})C\ ^2\Sigma_g^+$ partial-channel photoionization cross section obtained from the components of Fig. 6(a) is presented in Fig. 6(b) in comparison with measured values.[30,33,38-41] The experimental and theoretical results are apparently in good quantitative accord, except at higher energies, substantiating in large measure the shape and location of the $4\sigma_g \rightarrow 4\sigma_u$ (σ^*) diabatic intravalence feature in the $4\sigma_g \rightarrow k\sigma_u$ component of Fig. 6(a). This result is quite similar to the $4\sigma^{-1}$ cross section in CO (Ref. 59) although the resonance in that case is somewhat lower lying. The discrepancy between theory and experiment in the $(4\sigma_g^{-1})C\ ^2\Sigma_g^+$ channel above ~40 eV is tentatively attributed in the following subsection to coupling with inner-valence-shell $2\sigma_u^{-1}$ and $3\sigma_g^{-1}$ channels.

B. Inner-valence-shell cross sections

The calculated $2\sigma_u$ (σ) and $3\sigma_g$ (σ) inner-valence-shell excitation spectra are presented in Table VII, and corresponding photoionization cross sections are given in Fig. 7. The thresholds employed correspond to Koopmans values in these cases.

1. $2\sigma_u$ (σ) spectra (I.P. = 41.3 eV)

The $2\sigma_u \rightarrow n\sigma_g$ excitations of Table VII evidently form an $ns\sigma_g$ Rydberg series in good accord with quantum-defect estimates obtained using the large value $\delta = 1.4$. Evidently, the $5\sigma_g$ (σ^*) virtual valence orbital contributes to the $2\sigma_u \rightarrow k\sigma_g$ photoionization continuum of Fig. 7(a), where it appears just above threshold at ~42 eV, and presumably

TABLE VII. $2\sigma_u$ (I.P. = 41.3 eV) and $3\sigma_g$ (I.P. = 42.8 eV) excitation spectra in CO_2.

Present results[a] Energy (eV)/*f* number	Defect estimates[b] Energy (eV)/*f* number	Present results[a] Energy (eV)/*f* number	Defect estimates[b] Energy (eV)/*f* number
$(2\sigma_u)\ ^1\Sigma_g^+ \rightarrow (ns\sigma_g)\ ^1\Sigma_u^+$		$(3\sigma_g)\ ^1\Sigma_u^+ \rightarrow (np\sigma_u)\ ^1\Sigma_u^+$	
36.68/0.044 2	36.01/0.1428	40.61/0.000 32	40.19/
39.36/0.024 9	39.31/0.0333	41.67/0.000 01	41.51/
40.27/0.012 2	40.27/0.0125	42.10/	42.02/
40.68/0.006 6	40.68/0.0060	42.32/	42.28/
40.89/0.004 1	40.89/0.0033	42.51/	42.42/
41.20/	41.01/0.0022		
$(2\sigma_u)\ ^1\Sigma_g^+ \rightarrow (nd\pi_g)\ ^1\Pi_u$		$(3\sigma_g)\ ^1\Sigma_g^+ \rightarrow (np\pi_u)\ ^1\Pi_u$	
39.88/0.000 051	39.81/	36.06/0.008 62	
40.51/0.000 020	40.47/	40.09/0.000 30	40.19/0.001 12
40.80/0.000 010	40.78/	41.50/0.000 18	41.51/0.000 38
40.96/0.000 006	40.94/	42.02/0.000 10	42.02/0.000 17
41.19/	41.04/	42.28/0.000 06	42.28/0.000 09
		42.44/	42.42/0.000 05

[a] As in Table IV, employing Koopmans ionization potentials.

[b] As in Table IV, footnote c, employing quantum defects of $\delta = 1.4$, 0.7, and 0.0 for *ns*, *np*, and *nd* Rydberg series, respectively, for $n = 3, 4, \ldots$, and the threshold oscillator-strength values of Fig. 7. Because of the very small values of the oscillator-strength densities at threshold of Fig. 7, the *f* numbers for $nd\pi_g$ and $np\sigma_u$ excitations are not estimated reliably from the quantum-defect approximation, and so are not included in these cases.

also perturbs the Rydberg series. This channel is evidently highly similar to the $3\sigma_u$ excitation/ionization spectrum of Table VI and Fig. 4.

The $2\sigma_u \rightarrow n\pi_g$ excitations of Table VII evidently form a very weak $nd\pi_g$ Rydberg series, the positions of which are in good accord with quantum-defect estimates. Because the f numbers are so small it is not possible to obtain reliable quantum-defect estimates in this case. The corresponding $2\sigma_u \rightarrow k\pi_g$ cross section of Fig. 7(a) evidently contains a broad and relatively strong kd atomiclike feature centered at ~63 eV.

2. $3\sigma_g$ (σ) spectra (I.P. = 42.8 eV)

The $3\sigma_g \rightarrow n\sigma_u$ excitations of Table VII evidently form a very weak $np\sigma_u$ Rydberg series with most of the intensity in this channel found in the $3\sigma_g \rightarrow k\sigma_u$ cross section of Fig. 7(a). Since the f numbers are so small in this case it is not possible to obtain reliable quantum-defect estimates. The expected intense $3\sigma_g \rightarrow 4\sigma_u$ (σ^*) intravalence diabatic transition evidently contributes to the $3\sigma_g \rightarrow k\sigma_u$ cross section at ~60 eV.

The $3\sigma_g \rightarrow n\pi_u$ excitations of Table VII apparently included the expected $3\sigma_g \rightarrow 2\pi_u$ (π^*) transition, and an $np\pi_u$ Rydberg series in excellent accord with corresponding defect estimates. The $3\sigma_g \rightarrow k\pi_u$ cross section of Fig. 7(a) is consequently broad and weak but contains a feature that can be attributed to kd contributions.

3. Many-electron partial-channel cross section

Green's-function calculations in CO_2 indicate strong configuration mixing in the ionic states corresponding to inner-valence-shell ionization, and the corresponding photoelectron spectra show broad features designated as many-electron transitions.[54,55] These states are expected to borrow intensity primarily, but not entirely, from the inner-valence-shell $2\sigma_u$ (σ) and $3\sigma_g$ (σ) orbitals. Consequently, the sum of the intensities of the partial-channel cross sections obtained from $(e,2e)$ studies in the inner-valence-shell region are compared in Fig. 7(b) with the sum of the calculated $2\sigma_u$ (σ) and $3\sigma_g$ (σ) cross sections. Evidently, the experimental and theoretical results are in satisfactory agreement only at the highest energies for which measured data are available. The explicit effects of intensity borrowing, in which cognizance is taken of the thresholds of the correct ionic states, must evidently be incorporated in the theoretical development in order to improve agreement with experiment.[68] In addition, there may be coupling between the inner-valence-shell channels and the $(4\sigma_g^{-1})C\ ^2\Sigma_g^+$ scattering states in the ~40–55 eV interval [cf. Figs. 6(b) and 7(b)].

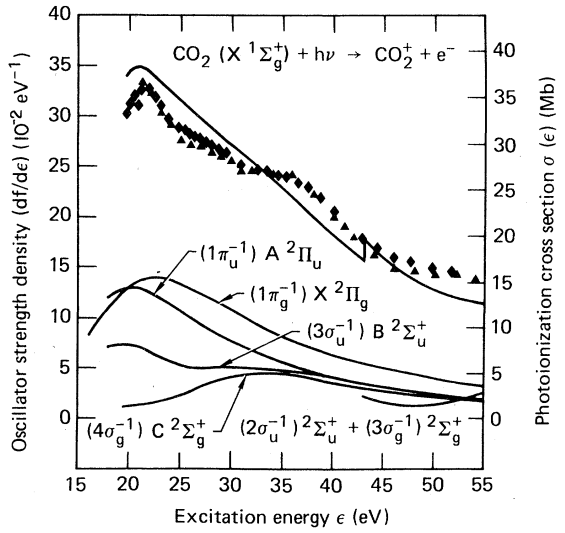

FIG. 8. Partial-channel and total photoionization cross sections in CO_2; (——), static-exchange results from Figs. 2 to 7; ▲, electron-impact data (Ref. 30); ♦, synchrotron radiation data (Ref. 15).

C. Valence-shell photoabsorption cross section

An additional comparison between theory and experiment is provided by total photoabsorption and electron energy-loss measurements in the 20 to 60 eV range.[15,30] In Fig. 8 are shown the six valence-shell partial-channel cross sections of Figs. 2 to 7 and their sum in comparison with total photoabsorption cross sections obtained from synchrotron radiation[15] and electron-impact measurements.[30] Evidently, the theoretical and experimental results are in very good quantitative accord. Note from Figs. 2(b) and 3(b), however, that an apparent compensation of errors makes the agreement between theory and experiment of Fig. 8 somewhat fortuitous at low energy. That is, the theoretically determined $(1\pi_g^{-1})X^2\Pi_g$ cross section apparently provides an overestimate at low energy, whereas the theoretically determined $(1\pi_u^{-1})A\ ^2\Pi_u$ cross section gives a compensating underestimate at low energy. Presumably channel coupling between $1\pi_g \rightarrow k\delta_u$ and $1\pi_u \rightarrow k\delta_g$ photoionization in the ~20 to 25 eV interval can account for these two compensating discrepancies, as indicated above. The $(4\sigma_g^{-1})C\ ^2\Sigma_g^+$ partial-channel contribution in the ~30 to 40 eV interval evidently gives rise to an inflection in both the theoretical and experimental results, and the inner-valence-shell contributions are also discernible in the total cross section at ~50 eV. As in the case of $1\pi_g$ and $1\pi_u$ ionization, there is evidently a compensation of errors in the $4\sigma_g^{-1}$ and inner-valence-shell channels, as indicated above. The two independently obtained experimental results of Fig. 8 are

TABLE VIII. $2\sigma_g$ (I.P. = 297.5 eV), $1\sigma_u$ (I.P. 541.1 eV), and $1\sigma_g$ (I.P. = 541.1 eV) excitation spectra in CO_2.

Present results[a] Energy (eV)/f number	Defect estimates[b] Energy (eV)/f number	Present results[a] Energy (eV)/f number	Defect estimates[b] Energy (eV)/f number
$(2\sigma_g)\,^1\Sigma_g^+ \rightarrow (n\sigma_u)\,^1\Sigma_u^+$		$(2\sigma_g)\,^1\Sigma_g^+ \rightarrow (n\pi_u)\,^1\Pi_u$	
295.38/0.000 418	294.93/0.000 358	282.98/0.250 9	
296.42/0.000 121	296.25/0.000 121	294.53/0.003 2	294.93/0.006 7
296.85/0.000 047	296.76/0.000 055	296.15/0.001 5	296.25/0.002 3
297.07/0.000 022	297.02/0.000 029	296.73/0.000 7	296.76/0.001 0
297.26/	297.16/0.000 017	297.00/0.000 4	297.02/0.000 5
		297.14/	297.16/0.000 3
$(1\sigma_u)\,^1\Sigma_g^+ \rightarrow (n\sigma_g)\,^1\Sigma_u^+$		$(1\sigma_u)\,^1\Sigma_g^+ \rightarrow (n\pi_g)\,^1\Pi_u$	
534.28/0.039 0		539.61/0.002 43	539.59/0.003 02
538.51/0.012 1	538.29/0.011 5	540.20/0.001 22	540.25/0.001 28
539.81/0.004 0	539.77/0.003 7	540.56/0.000 66	540.56/0.000 65
540.34/0.001 7	540.33/0.001 7	540.73/0.000 41	540.72/0.000 38
540.60/0.000 9	540.60/0.000 9	540.94/	540.82/0.000 24
540.80/	540.75/0.000 5		
$(1\sigma_g)\,^1\Sigma_g^+ \rightarrow (n\sigma_u)\,^1\Sigma_u^+$		$(1\sigma_g)\,^1\Sigma_g^+ \rightarrow (n\pi_u)\,^1\Pi_u$	
538.78/0.000 632	538.53/0.000 671	531.98/0.129 7	
539.96/0.000 201	539.85/0.000 227	538.49/0.000 90	538.53/0.001 12
540.42/0.000 080	540.36/0.000 103	539.86/0.000 35	539.85/0.000 38
540.65/0.000 047	540.62/0.000 055	540.37/0.000 16	540.36/0.000 17
540.83/	540.75/0.000 033	540.62/0.000 09	540.62/0.000 09

[a] As in Table IV, employing the experimentally determined ESCA ionization thresholds (Ref. 83).

[b] As in Table IV, footnote c, employing quantum defects of $\delta = 0.7$, 0.7, and 0.0 for ns, np, and nd series, respectively, for $n = 3, 4, \ldots$, and the threshold oscillator-strength values of Figs. 9(a) and 10(a).

[c] Electron-impact studies of the carbon and oxygen K-edge spectra show peaks at 290.7, 292.7, 294.5, 294.6, and 296.3 eV, and at 535.4, 538.7, 539.9, and 540.8 eV, respectively (Ref. 19).

evidently in very good mutual agreement, and the theoretical calculations clarify completely the origins of the various features in the partial-channel components that comprise the total cross section.

D. K-edge cross sections

The $2\sigma_g$ (C1s), $1\sigma_u$ (O1s), and $1\sigma_g$ (O1s) excitation series are shown in Table VIII, and the corresponding photoionization cross sections are given in Figs. 8 and 9. Experimental estimates of 297.5 and 541.1 eV are employed as the appropriate carbon and oxygen ionization thresholds, respectively.[83]

1. $2\sigma_g$ (C1s) spectra (I.P. = 297.5 eV)

The $2\sigma_g \rightarrow n\sigma_u$ excitations of Table VIII evidently form a weak $np\sigma_u$ Rydberg series, with much of the intensity in this channel appearing in the form of a $2\sigma_g \rightarrow 4\sigma_u$ (σ^*) resonance above threshold in the $2\sigma_g \rightarrow k\sigma_u$ cross section of Fig. 9(a). By contrast, there is a strong $2\sigma_g \rightarrow 2\pi_u$ (π^*) intravalence transition in the discrete $2\sigma_g \rightarrow np\pi_u$ excitations of Table VIII, and the corresponding $2\sigma_u \rightarrow k\pi_u$ continuum of Fig. 8(a) is broad and relatively weak. The calculated position of the $2\sigma_g \rightarrow 2\pi_u$ (π^*) intravalence transition is in poor accord with the measured value at 290.7 eV,[19] presumably as a consequence of the sensitivity of such transitions in K-edge spectra to the effects of orbital relaxation and correlation.[57] Similarly, the calculated $np\pi_u$ and $np\sigma_u$ Rydberg excitations are in somewhat better but only general accord with the measured values.[19]

The $2\sigma_g$ photoionization components of Fig. 9(a) and compared with the experimental cross section obtained from electron-impact measurements in Fig. 9(b).[19] There is evidently only general agreement between the two results, and the $2\sigma_g \rightarrow 4\sigma_u$ (σ^*) feature above threshold is apparently split into two peaks by the effects of configuration interaction in the ionic states. Note that the mea-

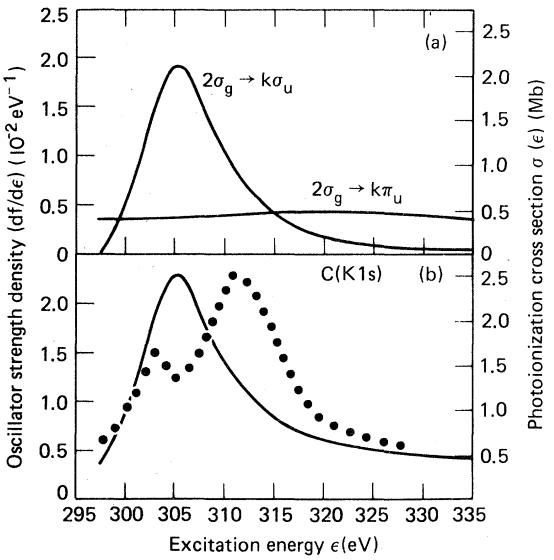

FIG. 9. (a) As in Fig. 2(a) for $2\sigma_g \rightarrow k\sigma_u$ and $k\pi_u$ photoionization; (b) as in Fig. 2(b) for C1s K-edge photoionization in CO_2; •, electron-impact data (Ref. 19) normalized to the calculated values at ~300 eV.

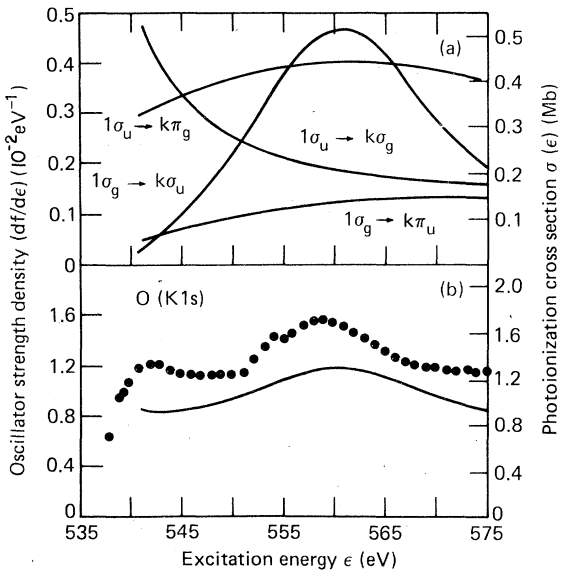

FIG. 10. (a) As in Fig. 2(a) for $1\sigma_u \rightarrow k\sigma_g$ and $k\pi_g$ and $1\sigma_g \rightarrow k\sigma_u$ and $k\pi_u$ photoionization; (b) as in Fig. 2(b) for O1s K-edge photoionization in CO_2; •, absorption data (Ref. 34).

sured relative data is normalized to the calculated cross section at ~300 eV. There is some similarity between the results of Fig. 9 and the previously reported carbon K-edge cross section in CO.[59]

2. $1\sigma_u$ (O1s) spectra (I.P. = 541.1 eV)

The $1\sigma_u \rightarrow n\sigma_g$ excitations of Table VIII evidently include a relatively strong $1\sigma_u \rightarrow 5\sigma_g$ (σ^*) transition, as well as an $ns\sigma_g$ Rydberg series having the relatively small defect of $\delta = 0.7$. A similar defect is also appropriate for the $1\sigma_u \rightarrow n\pi_g$ excitations, which evidently comprise an $nd\pi_g$ Rydberg series. The $1\sigma_u \rightarrow 5\sigma_g$ (σ^*) resonance may contribute to the experimentally assigned transition at 535.4 eV,[19] and clearly perturbs the $ns\sigma_g$ Rydberg series.

The $1\sigma_u \rightarrow k\sigma_g$ photoionization cross section of Fig. 10(a) has a relatively large value at threshold, apparently due to the $5\sigma_g$ (σ^*) diabatic contribution, which is largely localized in the discrete transitions. A broad kd feature evidently dominates the $1\sigma_u \rightarrow k\pi_g$ cross section, which is seen to be relatively strong.

3. $1\sigma_g$ (O1s) spectra (I.P. = 541.1 eV)

The $1\sigma_g \rightarrow n\sigma_u$ excitations of Table VIII evidently comprise an $np\sigma_u$ Rydberg series having a quantum defect of $\delta = 0.7$ with no evidence of the $4\sigma_u$ (σ^*) virtual orbital present in the spectrum. Rather, this feature appears in the $1\sigma_g \rightarrow k\sigma_u$ photoionization cross section of Fig. 10(a) as a diabatic resonancelike contribution centered at ~560 eV.

An expected intense $1\sigma_g \rightarrow 2\pi_u$ (π^*) transition appears in the $1\sigma_g \rightarrow n\pi_u$ excitations, with the higher members forming an $np\pi_u$ Rydberg series with defect $\delta = 0.7$. Since much of the intensity in this channel appears in the discrete spectral region, the corresponding $1\sigma_g \rightarrow k\pi_u$ photoionization cross section of Fig. 10(a) is relatively weak. The position of the $1\sigma_g \rightarrow 2\pi_u$ (π^*) resonance is only in general accord with the measured value of 535.4 eV (Ref. 19) presumably as a consequence of the neglect of core relaxation and correlation.

4. O(K1s) cross section

The measured oxygen K-edge absorption cross section in CO_2,[34] shown in Fig. 10(b), has features at ~542 and 560 eV that can be assigned as $1\sigma_u \rightarrow 5\sigma_g$ (σ^*) and $1\sigma_g \rightarrow 4\sigma_u$ (σ^*) contributions, respectively. There is, however, a modest quantitative discrepancy between theory and experiment, and an additional feature at ~554 eV in the measured cross section is not accounted for by the present calculations. Nevertheless, it is quite clear from Fig. 10 that the static-exchange results clarify the origins of the doubled peaked structure in the oxygen K-edge cross section in CO_2.[34] These results differ from the previously reported oxygen K-edge cross section in CO due to the presence of the two σ^* valencelike virtual orbitals in CO_2, which are conveniently regarded as even [$5\sigma_g$ (σ^*)] and odd [$4\sigma_u$ (σ^*)] combinations of the C–O σ^* orbitals. Consequently, their positions in Fig.

10 just above and ~20 eV above thresholds are consistent with the position of the σ^* orbital in CO, which is ~10 eV above threshold.[59]

IV. CONCLUDING REMARKS

The vertical-electronic static-exchange photoexcitation and ionization cross sections reported here provide a first approximation to the complete dipole spectrum in carbon dioxide. Comparisons with spectral assignment and measured photoabsorption/ionization cross sections corresponding to summations over vibrational and rotational substructures indicate that the separate-channel static-exchange approximation is generally satisfactory in CO_2. There is evidence, however, of coupling between certain outer-valence-shell scattering states, and, as is generally the case in light diatomic and polyatomic molecules, ionic-core configuration interaction is important in the inner-valence-shell and, to a lesser extent, K-edge spectral regions. Since the calculations reported here employ L^2 methods familiar from bound-state investigations, the resulting discrete and continuum spectra can be discussed qualitatively employing the common perspective of molecular-orbital terminology.

It is found that the calculated discrete excitation spectra are generally comprised of Rydberg series in good accord with recent experimental assignments and include strong contributions from the virtual $2\pi_u$ (π^*) valence orbital. There is also evidence of strong $1\pi_u \rightarrow 5\sigma_g$ (σ^*) and $3\sigma_u \rightarrow 5\sigma_g$ (σ^*) intravalence contribution in the calculated discrete excitation spectra. These features contribute to a continuumlike structure in the measured electron-impact excitation spectrum at ~13.5 eV, and the former may result in photoproduction of CO in the $A\ ^1\Pi_u$ state. By contrast, the $4\sigma_g \rightarrow 2\pi_u$ (π^*) intravalence transition is found to be significantly higher lying on basis of the present calculations, in contrast to some previously reported calculations, whereas the $1\pi_g \rightarrow 2\pi_u$ (π^*) transition has been assigned previously at ~12.5 eV excitation energy. The calculated inner-valence-shell discrete excitation spectra are relatively weak, and there are apparently no spectral assignments available for comparison. Although the calculated carbon and oxygen K-edge excitations are in general accord with electron-impact excitation measurements, there are some quantitative discrepancies due to neglect of relaxation and correlation effects.

The various photoionization continua are generally dominated by diabatic $4\sigma_u$ (σ^*) and $5\sigma_g$ (σ^*) virtual valence orbitals, which give rise to resonancelike features having a strictly molecular origin. In addition, certain of the partial-channel cross sections contain $\delta_g d$, $\delta_u d$, and $\pi_g d$ features that are of apparent atomic origin, and presumably correlate with strongly allowed transitions in the separated-atom limits. Specifically, the $1\pi_g$ and $1\pi_u$ cross sections are seen to be dominated by strong $\delta_u d$ and $\delta_g d$ features, respectively, which presumably correlate with dipole allowed $2p \rightarrow kd$ transitions in the separated-atom limits. The presence of these features are verified by the measured partial-channel cross sections for production of $(1\pi_g^{-1})X\ ^2\Pi_g$ and $(1\pi_u^{-1})A\ ^2\Pi_u$ parent molecular ions, which show structures in good accord with the static-exchange calculations.

The $1\pi_g$ and $1\pi_u$ cross sections are qualitatively similar to previously reported corresponding cross sections in O_2, apparently as a consequence of the largely atomic oxygen $2p$ composition of the $1\pi_g$ and $1\pi_u$ orbitals in CO_2. As in O_2, there is evidence of coupling between $1\pi_g^{-1}k\delta_u$ and $1\pi_u^{-1}k\delta_g$ configurations, resulting in modest quantitative discrepancies between theory and experiment for the $X\ ^2\Pi_g$ and $A\ ^2\Pi_u$ channels over a portion of the spectrum.

The calculated $3\sigma_u$ and $4\sigma_g$ cross sections are found to be dominated by $5\sigma_g$ (σ^*) and $4\sigma_u$ (σ^*) resonancelike features, respectively, which are clearly discernible in the measured $(3\sigma_u^{-1})B\ ^2\Sigma_u^+$ and $(4\sigma_g^{-1})C\ ^2\Sigma_g^+$ partial-channel cross sections. Because of the presence of both $5\sigma_g$ (σ^*) and $4\sigma_u$ (σ^*) virtual valence orbitals in the CO_2 continuum, the $3\sigma_u$ (σ) and $4\sigma_g$ (σ) cross sections differ quantitatively from the previously studied 5σ and 4σ cross sections in CO. Indeed, the $5\sigma_g$ (σ^*) and $4\sigma_u$ (σ^*) resonances are conveniently regarded as even and odd combinations, respectively, of 6σ (σ^*) orbitals in the CO bonds, accounting for their appearance near and ~15–20 eV above threshold, respectively, in the CO_2 photoionization continua. By contrast, the 6σ (σ^*) feature in CO appears at a democratic ~10 eV above threshold.

Further evidence of the importance of the $5\sigma_g$ (σ^*) and $4\sigma_u$ (σ^*) diabatic contributions to the partial-channel cross sections in CO_2 is provided by the inner-valence-shell $2\sigma_u$ and $3\sigma_g$ profiles, which exhibit the appropriate structures. Because of the importance of ionic-core configuration interaction in the inner-valence-shell region, there is only general agreement with the measured partial-channel data in this region. Somewhat more detailed theoretical studies in this case are presently in progress. The calculated $2\sigma_u$ C($K1s$) and $1\sigma_{u,g}$ O($K1s$) K-edge cross sections also contain the expected $5\sigma_g$ (σ^*) and $4\sigma_u$ (σ^*) features, and the predicted positions are in good accord with available measured data. It if of interest to note that both $5\sigma_g$ (σ^*) and $4\sigma_u$ (σ^*) features appear in the calculated oxygen $(1\sigma_g, 1\sigma_u)$ K-edge cross sections,

in good agreement with photoabsorption measurements.

ACKNOWLEDGMENTS

It is a pleasure to acknowledge the support of the U.S.-Latin American Science Program, NSF(OIP)-CNPq (Brazil), of the Foundation for the Advancement of Science of the State of São Paulo (FAPESP), of the Donors of the Petroleum Research Fund administered by the American Chemical Society, and of the NASA Ames Research Center through the auspices of the U.S. National Research Council.

---

*Permanent address.

[1]S. Mrozowski, Phys. Rev. 72, 691 (1947).

[2]E. C. Y. Inn, K. Watanabe, and M. Zelikoff, J. Chem. Phys. 21, 1648 (1953).

[3]Y. Tanaka, A. S. Jursa, and F. J. LeBlanc, J. Chem. Phys. 32, 1199 (1960).

[4]Y. Tanaka and M. Ogawa, Can. J. Phys. 40, 879 (1962).

[5]R. B. Cairns and J. A. Samson, J. Geophys. Res. 70, 99 (1965).

[6]R. C. Nakata, K. Watanabe, and F. M. Matsunaga, Sci. Light (Tokyo) 14, 54 (1965).

[7]G. R. Cook, P. H. Metzger, and M. Ogawa, J. Chem. Phys. 44, 2935 (1966).

[8]V. A. Koryoshkin, Dok. Akad. Nauk. SSR 167, 1035 (1966) [Sov. Phys.–Dokl. 11, 329 (1966).

[9]J. Collins, Mem. Soc. R. Sci. Liege, Vol. 14, Hors Ser. 5, 1 (1967).

[10]J. D. Carette, Can. J. Phys. 45, 2931 (1967).

[11]D. Villarejo, R. Stockbauer, and M. G. Inghram, J. Chem. Phys. 48, 3342 (1968).

[12]J. W. Rabalais, J. M. McDonald, V. Scherr, and S. P. McGlynn, Chem. Rev. 71, 73 (1971).

[13]G. M. Lawrence, J. Chem. Phys. 56, 3435 (1972).

[14]K. E. McCulloh, J. Chem. Phys. 59, 4250 (1973).

[15]L. C. Lee, R. W. Carlson, D. L. Judge, and M. Ogawa, J. Quant. Spectrosc. Radiat. Transfer 13, 1023 (1973).

[16]F. R. Greening and G. W. King, J. Mol. Spectrosc. 59, 312 (1976).

[17]E. N. Lassettre, A. Skerbele, M. A. Dillon, and K. J. Ross, J. Chem. Phys. 48, 5066 (1968).

[18]M. Kraus, S. R. Mielczarek, D. Neumann, and C. E. Kuyatt, J. Geophys. Res. 76, 3733 (1971).

[19]V. Y. Foo, C. E. Brion, and J. B. Hasted, Proc. R. Soc. London Ser. A 322, 535 (1971); G. R. Wight and C. E. Brion, J. Electron Spectrosc. Relat. Phenom. 3, 191 (1974).

[20]R. Spohr and E. Von Puttkamer, Z. Naturforsch. 22A, 705 (1967).

[21]D. W. Turner, C. Baker, A. D. Baker, and C. R. Brundle, *Molecular Photoelectron Spectroscopy* (Wiley, New York, 1970).

[22]C. J. Allan, U. Gelius, D. A. Allison, G. Johansson, H. Siegbahn, and K. Siegbahn, J. Electron. Spectrosc. 1, 131 (1972).

[23]T. A. Carlson and G. E. McGuire, J. Electron Spectrosc. 1, 209 (1972).

[24]J. L. Bahr, A. J. Blake, J. H. Carver, J. L. Gardner, and V. Kumar, J. Quant. Spectrosc. Radiat. Transfer 12, 59 (1972).

[25]A. W. Potts and T. A. Williams, J. Electron Spectrosc. 3, 3 (1974).

[26]U. Gelius, J. Electron Spectrosc. 5, 983 (1974).

[27]C. E. Brion and D. S. C. Yee, J. Electron Spectrosc. 12, 77 (1977).

[28]D. A. Allison and R. G. Cavell, J. Chem. Phys. 68, 593 (1978).

[29]A. Giardini-Guidoni, R. Tiribelli, D. Vinciguerra, R. Camilloni, and G. Stefani, J. Electron Spectrosc. 12, 405 (1977).

[30]C. E. Brion and K. H. Tan, Chem. Phys. 34, 141 (1978).

[31]A. P. Hitchcock, C. E. Brion, and M. J. van der Wiel, Chem. Phys. Lett. 66, 213 (1979); Chem. Phys. 45, 461 (1980).

[32]R. E. LaVilla, J. Chem. Phys. 63, 2733 (1975).

[33]T. Gustafsson, E. W. Plummer, D. E. Eastman, and W. Gudat, Phys. Rev. A 17, 175 (1978).

[34]D. M. Barrus, R. L. Blake, A. J. Burek, K. C. Chambers, and A. L. Pregenzer, Phys. Rev. A 20, 1045 (1979).

[35]L. C. Lee and D. L. Judge, J. Chem. Phys. 57, 4443 (1972).

[36]R. W. Carlson, D. L. Judge, and M. Ogawa, J. Geophys. Res. 78, 3194 (1973).

[37]L. C. Lee, R. W. Carlson, and D. L. Judge, J. Phys. B 9, 855 (1976).

[38]J. A. R. Samson and J. L. Gardner, J. Chem. Phys. 58, 3771 (1973).

[39]J. L. Gardner and J. A. R. Samson, J. Electron Spectrosc. 2, 259 (1973).

[40]J. A. R. Samson and J. L. Gardner, J. Geophys. Res. 78, 3663 (1973).

[41]J. A. R. Samson, Phys. Rep. 4, 303 (1976).

[42]R. S. Mulliken, J. Chem. Phys. 3, 720 (1935).

[43]J. F. Mulligan, J. Chem. Phys. 19, 347 (1951).

[44]A. D. Mclean, J. Chem. Phys. 32, 1595 (1960).

[45]S. D. Peyerimhoff, R. J. Buenker, and J. L. Whitten, J. Chem. Phys. 46, 1707 (1967).

[46]C. W. McCurdy, Jr. and V. McKoy, J. Chem. Phys. 61, 2820 (1974).

[47]N. W. Winter, C. F. Bender, and W. A. Goddard, Chem. Phys. Lett. 20, 489 (1973).

[48]W. R. England, B. J. Rosenberg, P. J. Fortune, and A. C. Wahl, J. Chem. Phys. 65, 684 (1976).

[49]W. England, W. C. Ermler, and A. C. Wahl, J. Chem. Phys. 66, 2336 (1977).

[50]W. England, D. Yeager, and A. C. Wahl, J. Chem. Phys. 66, 2344 (1977).

[51]E. Lindholm, Ark. Fys. 40, 125 (1969).

[52]C. Fridh, L. Åsbrink, and E. Lindholm, Chem. Phys. 27, 169 (1978).

[53]W. von Niessen, G. H. E. Diercksen, and L. S. Cederbaum, J. Chem. Phys. 67, 4124 (1977).

[54]L. S. Cederbaum, J. Schirmer, W. Domke, and W. von Niessen, J. Phys. B 10, L549 (1977).

[55]W. Domcke, L. S. Cederbaum, J. Shirmer, W. von

Niessen, C. E. Brion, and K. H. Tan, Chem. Phys. 40, 171 (1979).
[56]W. Thiel and A. Schweig, Chem. Phys. Lett. 16, 409 (1972); M. S. Yurev and V. S. Yarunin, Opt. Spectrosc. 39, 672 (1975) [Opt. Spectrosc. (USSR) 39, 378 (1975)].
[57]T. N. Rescigno and P. W. Langhoff, Chem. Phys. Lett. 51, 65 (1977).
[58]T. N. Rescigno, C. F. Bender, B. V. McKoy, and P. W. Langhoff, J. Chem. Phys. 68, 970 (1978).
[59]N. Padial, G. Csanak, B. V. McKoy, and P. W. Langhoff, J. Chem. Phys. 69, 2992 (1978).
[60]A. Orel, T. N. Rescigno, B. V. McKoy, and P. W. Langhoff, J. Chem. Phys. 72, 1265 (1979).
[61]A. Gerwer, C. Asaro, B. V. McKoy, and P. W. Langhoff, J. Chem. Phys. 72, 713 (1980).
[62]P. W. Langhoff, A. Gerwer, C. Asaro, and B. V. McKoy, Int. J. Quantum Chem. S13, 645 (1979).
[63]T. N. Rescigno, A. Gerwer, B. V. McKoy, and P. W. Langhoff, Chem. Phys. Lett. 66, 116 (1979).
[64]P. W. Langhoff, S. R. Langhoff, and C. T. Corcoran, J. Chem. Phys. 67, 1722 (1977).
[65]P. W. Langhoff, A. E. Orel, T. N. Rescigno, and B. V. McKoy, J. Chem. Phys. 69, 4689 (1978).
[66]Geoffry R. J. Williams and P. W. Langhoff, Chem. Phys. Lett. 60, 201 (1978).
[67]N. Padial, G. Csanak, B. V. McKoy, and P. W. Langhoff, J. Chem. Phys. (to be published).
[68]P. W. Langhoff, S. R. Langhoff, T. N. Rescigno, J. Shirmer, L. S. Cederbaum, W. Domke, and W. von Niessen, Chem. Phys. (to be published).
[69]P. W. Langhoff, in *Electron-Molecule and Photon-Molecule Collisions*, edited by T. N. Rescigno, B. V. McKoy and B. Schneider (Plenum, New York, 1979), pp. 183–224.
[70]P. W. Langhoff, in *Proceedings of the International Conference on Moment Methods in Many-Fermion Systems*, edited by B. J. Dalton, S. M. Grimes, J. P. Vary, and S. A. Williams (Plenum, New York, 1980), pp. 191–212.
[71]T. H. Dunning and J. P. Hay, in *Modern Theoretical Chemistry*, edited by H. F. Schaefer III (Plenum, New York, 1976), Vol. 3, Chap. 1.
[72]H. F. Schaefer III, *The Electronic Structure of Atoms and Molecules* (Addison-Wesley, Reading, Mass., 1972).
[73]This simple but fundamental point is obscured in the otherwise useful review of W. P. Reinhardt, Comput. Phys. Commun. 17, 1 (1979), who incorrectly asserts that the Stieltjes moment approach (Ref. 69) and an approximate mapping of the variational pseudospectrum [Eq. (3)] on a classical quadrature (a well-known reference density technique, Ref. 74) are in principle equivalent. Our experience with smoothing literally hundreds of highly irregular variationally determined pseudospectra (Refs. 57–70) indicates that construction of moment-theory spectra [Eq. (4)] is a necessary preliminary to successfully extracting underlying photoionization cross sections. By contrast, Reinhardt observes that the mapping approach can be more stable in practice than the moment analysis, perhaps as a consequence of his restricting applications largely to model and one-electron problems, in which cases the variationally determined pseudospectra are generally smooth.
[74]C. T. Corcoran and P. W. Langhoff, Chem. Phys. Lett. 41, 609 (1976).
[75]P. W. Langhoff, C. T. Corcoran, J. S. Sims, F. Weinhold, and R. G. Glover, Phys. Rev. A 14, 1042 (1976).
[76]C. T. Corcoran and P. W. Langhoff, J. Math. Phys. 18, 651 (1977).
[77]J. C. Slater, *Electronic Structure of Molecules* (McGraw-Hill, New York, 1963).
[78]T. S. Wauchop and H. P. Broida, J. Geophys. Res. 76, 21 (1971).
[79]W. Sroka and R. Zeitz, Phys. Lett. 43A, 493 (1973).
[80]E. P. Gentieu and J. E. Mentall, J. Chem. Phys. 64, 1376 (1976).
[81]J. H. D. Eland, M. Devoret, and S. Leach, Chem. Phys. Lett. 43, 97 (1976).
[82]It is of some interest to note in connection with possible crossover from B to A states in CO_2^+ (Ref. 40) that quantum yields in emission greater than (1.8) and less than (0.54) unity, respectively, are reported in these cases at 21.2 eV (Ref. 81). Such a crossover, if present, as the quantum-yield measurements apparently suggest, would invalidate the equivalence of fluorescence-production and partial-channel photoionization cross sections. Consequently, it is important to recognize that interpretation of the quantum-yield experiments (Ref. 81) requires photoionization branching ratios for the appropriate states. Use of the branching ratios calculated here, rather than those obtained from PES measurements, in conjunction with the measured data (Ref. 81) gives quantum yields in emission of approximate unity for both A and B states in CO_2^+.
[83]K. Siegbahn, C. Nordling, G. Johansson, J. Hedman, P. F. Heden, K. Hamrin, U. Gelius, T. Bergmark, L. O. Werme, R. Manne, and Y. Baer, *ESCA Applied to Free Molecules* (North-Holland, Amsterdam, 1969).